Uniform description of bulk observables in the hydrokinetic model of $A + A$ collisions at the BNL Relativistic Heavy Ion Collider and the CERN Large Hadron Collider

Iu. A. Karpenko,[1,2] Yu. M. Sinyukov,[1] and K. Werner[3]

[1]*Bogolyubov Institute for Theoretical Physics, Metrolohichna Strasse 14b, 03680 Kiev, Ukraine*

[2]*Frankfurt Institute for Advanced Studies, Ruth-Moufang-Strasse 1, 60438 Frankfurt am Main, Germany*

[3]*SUBATECH, University of Nantes-IN2P3/CNRS-EMN, Nantes, France*

A simultaneous description of hadronic yields; pion, kaon, and proton spectra; elliptic flows; and femtoscopy scales in the hydrokinetic model of $A + A$ collisions is presented at different centralities for the top BNL Relativistic Heavy Ion Collider (RHIC) and CERN Large Hadron Collider (LHC) 2.76-TeV energies. The initial conditions are based on the Monte Carlo Glauber simulations. When going from RHIC to LHC energy in the model, the only parameters changed are the normalization of the initial entropy defined by the number of all charged particles in most central collisions, contribution to entropy from binary collisions, and barionic chemical potential. The hydrokinetic model is used in its hybrid version, which provides the correct match (at the isochronic hypersurface) of the decaying hadron matter evolution with hadronic ultrarelativistic quantum molecular dynamics cascade. The results are compared with the standard hybrid models where hydrodynamics and hadronic cascade are matching just at the non-space-like hypersurface of chemical freeze-out or on the isochronic hypersurface. The modification of the particle-number ratios at LHC caused, in particular, by the particle annihilations at the afterburn stage is also analyzed.

PACS number(s): 13.85.Hd, 25.75.Gz, 24.10.Jv, 24.10.Nz

I. INTRODUCTION

Soon after the first CERN Large Hadron Collider (LHC) heavy ion results were launched, it became evident that the hydrodynamic picture of the collision processes, confirmed at BNL Relativistic Heavy Ion Collider (RHIC), is clearly seen also at much higher energy. This conclusion is based on two classes of observables. The first one is related to the azimuthal anisotropy of particle spectra expressed basically through its second harmonics, or v_2 coefficients. The obtained LHC results for the transverse momentum dependence of $v_2(p_T)$ at a given centrality bin were found to be similar to the ones at RHIC, except for the higher momentum range at LHC [1]. This is the evidence of the same hydrodynamic mechanism of the anisotropy formation as at RHIC. The second type of observables deals with the direct measurements of the space-time structure of nucleus-nucleus collisions by means of the correlation femtoscopy. The femtoscopic spatiotemporal scales of the systems are typically represented in terms of the interferometry radii. The hydrodynamic predictions [2] for p_T behavior of the radii at the LHC energies were confirmed by the ALICE experiment [3]. The most impressive hydrodynamic prediction [4,5], that the ratio of the two transverse interferometry radii, *out* to *side*, will drop in the whole p_T interval with increasing collision energy and reaches a value close to unity at the LHC, has been discovered experimentally [3].

Now the hydrodynamic-based approach to ultrarelativistic nucleus-nucleus collisions becomes the "standard model" for these processes. Note, however, that the details of this approach did undergo essential modifications during the last decade and even now they are different in different models. The first attempts to describe successfully v_2 coefficients [6] at RHIC were based on the perfect hydrodynamics with an equation of state (EoS) corresponding to a first-order phase transition. However, a simultaneous description of v_2, particle spectra and femtoscopy scales within the unified initial conditions collided with an invincible problem. Only in recent years have the main factors that make it possible to describe simultaneously the spectra and femtoscopic scales become clear. They are [7–11] a relatively hard EoS because of a crossover transition (instead of the first-order one) between quark-gluon and hadron phases, the presence of the prethermal anisotropic transverse flow developed to thermalization time, an "additional portion" of the transverse flow caused by the shear viscosity effect, and fluctuations of the initial conditions. An account of these factors gives the possibility to describe well the pion and kaon spectra together with the femtoscopy RHIC data within a realistic freeze-out picture with a gradual decay of the fluid into observed particles [12].

In fact, at the moment there is no real unique model of heavy ion collisions: Different hydrodynamic-based approaches use different initial conditions as well as different final-state treatments for the matter evolution, different EoS, etc. In this paper we make the next step towards converging to the "standard model." We analyze a possibility for a uniform description of the soft observables in the hydrokinetic model of $A + A$ collisions at RHIC and LHC, namely, a simultaneous description of the hadronic yield; pion, kaon, and proton transverse momentum spectra at different centralities; $v_2(p_T)$ coefficients; and femtoscopy scales in $A + A$ collisions at RHIC and LHC. For this aim we use the hydrokinetic model (HKM) [8,12,13] in its hybrid version (hHKM) [14], which allows one to apply hydrodynamics also at the late nonequilibrated stage of gradual system decay. It gives the possibility to switch correctly to the ultrarelativistic quantum molecular dynamics (UrQMD) cascade at any spacelike hypersurface, in particular,

at an isochronic one. We can compare the results also with a pure hybrid model where the hydrodynamics and hadronic cascade are matching just at a non-space-like hypersurface of the chemical freeze-out or on the isochronic hypersurface. The goal of this paper is to fix the HKM by applying it to describe the known experimental data at RHIC and LHC and based on this to predict still unmeasured observables. The results presented here are correlated with similar studies performed in other hydrobased models, different from hHKM in various aspects [15–17].

II. MODEL DESCRIPTION

A. Initial conditions

All the results presented in this work are calculated for the midrapidity region with the approximation of longitudinal boost invariance. The hydrokinetic code [12] is developed now to simulate the full $3 + 1$D matter evolution and it allows one to analyze the central, noncentral, and peripheral heavy ion collisions. The formation of the flow anisotropy depends on the initial eccentricity ϵ which is defined by the centrality of collisions. Even at the maximal centrality the event-by-event fluctuations of the initial conditions (IC) lead to some nonzero effective eccentricity. These fluctuations appear to be attributable to chaotic distribution of nucleons (or local color charges) in colliding nucleus and, as the result, the nucleon scattering positions fluctuate from event to event. In the hydrodynamic picture such initial eccentricity of the (mean) energy density profile transforms into a flow anisotropy even at zero impact parameter. The effect persists for noncentral heavy ion collisions, where it leads to some systematic increase of mean initial eccentricity.

In this work, we employ the Monte Carlo Glauber (MC-Glauber) ICs.

1. The Glauber initial transverse profile

The mean transverse density of nucleons in nuclei is defined as

$$T(\mathbf{x}_T) = \int_{-\infty}^{\infty} \frac{a}{\exp\left[(\sqrt{x_L^2 + x_T^2} - R_A)/\delta\right] + 1} dx_L, \quad (1)$$

where A is the atomic number; for Au + Au collisions one uses $A = 197$, then $R_A = 1.12 A^{1/3} - 0.86 A^{-1/3} \approx 6.37$ fm, $\delta = 0.54$ fm. Constant a is defined by the normalization condition. In the so-called Glauber model the multiplicity (or entropy) produced in collisions of two nucleus is defined, roughly, by the number of participating nucleons contained in the overlapping distributions (1) for each nuclei shifted by the value of the impact parameter. In the MC-Glauber approach, instead of utilization of the mean participant density (1), one starts the Monte Carlo procedure with Eq. (1) as the distribution function of the random variable-nucleon number at point x_T. The finite size of the nucleon can also be taken into account; this slightly modifies the average nucleon distribution compared to Eq. (1). The collision criterion for a pair of nucleons in each event is based on the value of nucleon-nucleon cross section σ_{NN} at the corresponding collision energy. The nucleon-nucleon collisions result in deposition of a certain amount of multiplicity (entropy) to different cells in a transverse plane. The contributions to multiplicity (entropy) from the "hard" elementary collisions and from the "soft" ones are different: The former are proportional to the number of binary collisions while the later are associated with the number of wounded nucleons, or participant number [18]. The GLISSANDO code [19] allows one to calculate the x_T distribution of both numbers utilizing the MC-Glauber procedure. We use this generator and suppose that the initial entropy profile in the transverse plane at midrapidity is proportional to a linear combination of the density of wounded nucleons and that of binary collisions:

$$s(x_T) = C\left(\frac{1 - \delta}{2}\frac{dN_{\mathrm{w}}}{d^2 x_T} + \delta\frac{dN_{\mathrm{bin}}}{d^2 x_T}\right), \quad (2)$$

where C is the normalization constant, $\delta = 0.14$ for top RHIC energy, and $\delta = 0.08$ for 2.76-TeV LHC energy are fixed from the description of centrality dependence of multiplicity of all charged hadrons at midrapidity $dN_{\mathrm{ch}}/d\eta$ in a hydro + cascade model [20,21].

The MC-Glauber model requires the (inelastic) nucleon-nucleon cross section σ and the number of the nucleons $N_{\mathrm{a,b}}$ in the colliding nuclei as input. We fix this to ($\sigma = 42$ mb, $N_{\mathrm{a,b}} = 197$) for Au + Au collisions for top RHIC energy and ($\sigma = 64$ mb, $N_{\mathrm{a,b}} = 208$) for the LHC case. Different centrality classes are defined via the corresponding cuts on the number of participants, as shown in Table I. The other choice is to introduce cuts on impact parameter instead (which is associated with a cut on average number of participants); however, we found that it does not lead to visually different profiles.

Because we do not employ event-by-event hydrodynamics here, we average the profiles from a large-enough ensemble of events for each centrality class. The statistical fluctuations tilt in each event the principal axes of the ellipse of inertia and shift the center of mass relative to the reaction-plane coordinate system. To account for this effect, we superpose the principal axes by rotation and recentering of each initial distribution and after that take averages over the ensemble of events (so-called variable geometry analysis, also implemented as an option in

TABLE I. Cuts on the number of participating nucleons from MC-Glauber model, corresponding to different centrality classes for Au + Au and Pb + Pb collisions at top RHIC and 2.76-TeV LHC energies, respectively.

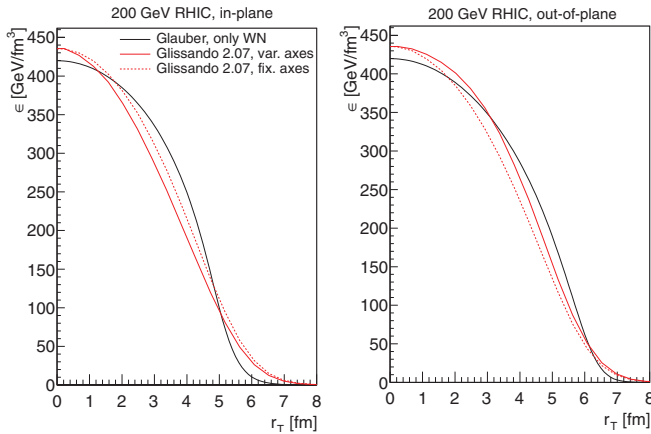| c (%)	0–5	5–10	10–20	20–30	30–40	$\cdots$
AuAu, RHIC	>328	328–279	279–201	201–143	143–98	$\cdots$
PbPb, LHC	>360	360–309	309–225	225–161	161–111	$\cdots$

FIG. 1. (Color online) The initial energy density profile along transverse x/in-plane (left) and y/out-of-plane (right) directions in the classical Glauber model (black curve) versus the MC-Glauber model with variable-axes analysis (solid red curve) and fixed-axes analysis (dashed red curve). For the MC-Glauber case, $\delta = 0.14$ is used in Eq. (2).

GLISSANDO code). This gives us nonzero initial eccentricity as a consequence of fluctuations, even for simulations with zero impact parameter. The resulting averaged distribution is then associated with the initial entropy density for hydrodynamic evolution.

In Fig. 1 we show the resulting energy density profiles for 0%–5% centrality collisions at the top RHIC energy from the MC-Glauber model, compared to the profile from classical Glauber. Note that the second term in Eq. (2), corresponding to a contribution from binary collisions, leads to a squeezed energy-density profile, which results in the increased radial flow in the system. At the same time, additional initial eccentricity (compared to the classical Glauber model) is gained mostly by performing the variable geometry analysis.

2. Initial time and transverse flow

In the hydrodynamic approach the initial entropy (or energy) density profile should be attributed to the initial time τ_i when (partial) thermalization is established. At this moment the system gains anisotropic prethermal transverse flow that is caused by the transverse finiteness of the system [7,9]. Typically the flow is almost nonrelativistic, $v_T \approx y_T$, and for the Gaussian initial profile for freely expanding fields or partons, which are suddenly thermalized at the time τ_i, is proportional to the transverse coordinate r and inversely proportional to the homogeneity lengths squared [9]. If the homogeneity length is directed along an axis that is tilted by angular ϕ to the in-plane axis x, then one can write it in the form

$$y_T = \alpha \frac{r_T}{R^2(\phi)}. \tag{3}$$

Naturally, the developing of the prethermal flows are different from that in hydrodynamic or free-streaming scenarios because of the different mechanisms of the flow generation at

the prethermal and thermal stages. The initial velocity profile is also different from Eq. (3) because of non-Gaussian initial energy distributions. The utilization of the method [22] to the thermalization processes in $A + A$ collisions at RHIC and LHC, which are neither hydrodynamical nor suddenly thermalized free-streaming ones, is in progress now. However, in this work we use a very rough approximation of ideal hydrodynamic evolution for the prethermal stage. This stage should start from the very initial time of the collision process, just after the center-of-mass (frame) energy in the overlapping region of colliding nucleus exceeds the binding energy, say at $\tau_0 = 0.1$ fm/c; this time has to be used in a consistent approach.

At initial time $\tau_0 = 0.1$ fm/c there is no collective transverse flow and our basic analysis is related just to this case. In addition, in Sec. III C we demonstrate the possible corrections caused by the modifications of the final radial and elliptic hydrodynamic flows, which are qualitatively similar to a corresponding effect caused by the shear viscosity.

B. Hydrodynamic evolution and equation of state in the chemically equilibrated zone

The quark-gluon plasma and hadronic gas are supposed to be in complete local equilibrium above the chemical freeze-out temperature T_{ch} with EoS at high temperatures as in the lattice QCD. With the given ICs, the evolution of thermally and chemically equilibrated matter is described with the help of the ideal hydrodynamic approximation. The latter is based on $3 + 1$D (in the general case) numerical hydrodynamic code, described in Ref. [12]. For this stage of evolution we use the latticeQCD-inspired EoS of the quark-gluon phase [23] together with corrections for small, but nonzero baryon chemical potentials [12,24], matched with chemically equilibrated hadron-resonance gas via crossover-type transition. The hadron-resonance gas consists of all ($N = 329$) well-established hadron states made of u, d, s quarks, including σ meson [$f_0(600)$]. Quantitatively, the EoS table used is not visually different from widely used s95p EoS parametrization [25,26], which isus based on results from the hotQCD collaboration [27,28].

C. Hydrokinetic and UrQMD cascade stages

At the temperatures below T_{ch} the system loses chemical and thermal equilibrium and gradually decays. In the hydrokinetic approach the dynamical decoupling is described by the particle escape probabilities in inhomogeneous hydrodynamically expanding systems in a way consistent with the kinetic equations in the relaxation-time approximation for emission functions [8,12]. The method allows one, in principle, to take into account the backreaction of the particle emission on the system evolution, which is, however, a fairly complicated technical procedure that is equivalent to viscous hydrodynamics only at small deviations from local equilibrium, and we do not apply it. However, without accounting for the backreaction, serious corrections of the emission function at large times are needed. It can be shown that the hydrokinetic approach

without such corrections results in overestimated effective temperature of proton spectra at RHIC energy and not enough rise of interferometry radii and volume from top RHIC to LHC energies [14]. To solve this problem we do not employ in this work the hydrokinetic approach at large times until free-streaming of finally produced particles. Instead of this we switch over a hydrokinetic evolution of continuous medium to an evolution of particles within UrQMD hadronic cascade [29]. The model which matches the HKM and UrQMD we call hHKM.

1. The Cooper-Frye switching over hydrodynamics to UrQMD cascade

In the present analysis, we compare the two different approaches to match hadrodynamic and hadronic cascade stages. The first one is standard and corresponds to a sudden transition from the hydrodynamic regime to the UrQMD cascade. In this approach, the distribution of ith sort of hadrons at switching hypersurface is expressed through hydrodynamic and thermodynamic variables $u(x)$, $T(x)$, $\mu_i(x)$ by the Cooper-Frye formula [30]:

$$p^0 \frac{d^3 N_i}{p_T dp_T d\phi_p dy}$$
$$= \int_{\sigma_{sw}} f_i^{l.eq.}(pu(x), T(x), \mu_i(x))\theta(p^\mu n_\mu) p^\mu d\sigma_\mu, \quad (4)$$

where n^μ is the hypersurface normal unit four vector with a positively defined zero component $n^0 > 0$. The obtained distributions after the Monte Carlo procedure serve as an input for UrQMD cascade. It has been known for a long time that such a prescription leads to inconsistencies [31,32], if the switching hypersurface contains the non-space-like sectors, and so should be modified to exclude formally negative contributions to the particle number of the particles that move towards the fluid. A cut of the negative contributions[1] leads, in its turn, to loss of causality and distorts hydrodynamic evolution. In addition, the particles interacting within UrQMD can interact also with fluid, and this opacity effect has to be taken into account, but usually not. So, despite its technical simplicity, the Cooper-Frye prescription should be applied with caution.

The method of direct matching of hydrodynamics and UrQMD cascade with Cooper-Frye prescription at the chemical freeze-out hypersurface we call traditionally a "hybrid" model. The chemical freeze-out isotherms typically contain non-space-like parts that can affect the results for some observables, and we shall check how large the effect is, comparing the results with ones obtained at the hydrokinetic matching at an isochronic hyperesurface.

If the matching hypersurface that separates (pure) hydrodynamics and UrQMD cascade is isochronic, we call

this model a "hybrid-isochronic" one. In such a model the above-mentioned problems with non-space-like hypersurface are absent. However, if one uses an isochronic hypersurface to match the cascade and hydrodynamic stages, it can contradict to the obvious expectation that at the periphery of such a hypersurface any local equilibrium input to the cascade stage is not correct. The peripheral regions are spatially and temporally rather far from the freeze-out isotherm, have rather small temperatures, and thus cannot be described hydrodynamically. We compare the results of the "hybrid-isochronic" model with the hHKM approach because the latter allows one to match UrQMD with a decaying hydrodynamic system, having nonequilibrated particle distributions, at isochronic hypersurfaces and in this way to overcome all mentioned problems.

2. Matching of the hydrokinetic stage and hadronic cascade

To construct the matching between hydrokinetics and UrQMD one calculates the distribution function for each sort of hadron at the switching hypersurface. Using the technique of the integral form of the Boltzmann equation [8,12], one can express the UrQMD input as the collection of all particles that propagate freely from the points of their last collision or just from the point of their creation and do reach this hypersurface. Because the evolution time is the Bjorken proper time τ, the distribution is expressed naturally in hyperbolic coordinates. Then the input for UrQMD is constructed as

$$f_i(\tau, \vec{x}, \vec{p}) = f_i^{l.eq.}(\tau_0, \vec{x}^{(\tau_0)}(\tau), \vec{p})$$
$$\times \exp\left(-\int_{\tau_0}^{\tau} \tilde{R}_i(s, \vec{x}^{(s)}(\tau), \vec{p}) ds\right)$$
$$+ \int_{\tau_0}^{\tau} d\lambda \left[f_i^{l.eq.}(\lambda, \vec{x}^{(\lambda)}(\tau), \vec{p}) \tilde{R}_i(\lambda, \vec{x}^{(\lambda)}(\tau), \vec{p})\right.$$
$$+ \tilde{G}_i^{decay}(\lambda, \vec{x}^{(\lambda)}(\tau), \vec{p})\right] \cdot$$
$$\times \exp\left(-\int_{\lambda}^{\tau} [\tilde{R}_i(s, \vec{x}^{(s)}(\tau), \vec{p})\right.$$
$$+ \tilde{D}_i(s, \vec{x}^{(s)}(\tau), \vec{p})] ds\right), \quad (5)$$

where $\vec{x} = \{\vec{r}_T, \theta\}$, $\tau = \sqrt{t^2 - x_L^2}$ is the proper time, $m_T = \sqrt{m^2 + p_T^2}$ is the transverse mass, $\theta = \eta - y$, η is the space-time rapidity, and y is the particle rapidity; notation

$$x^{(s)}(\tau) = \left\{\theta^{(s)}(\tau), \vec{r}_T^{(s)}(\tau)\right\} \quad (6)$$
$$= \left\{sh^{-1}\left(\frac{\tau}{s} sh(\theta)\right), \vec{r}_T\right.$$
$$\left. -\frac{p_T}{m_T}(\tau ch\theta - \sqrt{s^2 + \tau^2 sh^2\theta})\right\} \quad (7)$$

is used.

The different terms in Eq. (5) are as follows: $\tilde{R}_i(\lambda, \vec{x}, \vec{p}) = \frac{p_\mu u^\mu}{m_T \cosh\theta} R_i^*(p, T)$ is the collision rate of the ith sort of hadrons with the rest of particles, $\tilde{G}_i^{decay}(\lambda, \vec{x}, \vec{p})$ is an income of particles into the phase-space point owing to resonance decays, and $\tilde{D}_i(\lambda, \vec{x}, \vec{p}) = \frac{m}{p^0 \cosh\theta} \Gamma_i$ is the decay rate of a given

---

[1]This cut is implemented by the additional factor $\theta(p^\mu n_\mu)$ in the right-hand side of Eq. (4), where n_μ is the normal vector to the switching hypersurface [33], or by more sophisticated factors preserving particle number flow through the hypersurface [31].

resonance. To calculate the collision rates, we assume meson-meson, meson-baryon, and baryon-baryon cross sections in a way similar to the UrQMD code [29].

The hydrokinetic approach allows one to build the (nonequilibrium) distribution function accounting for the above-mentioned effects on any hypersurface σ_{sw} that is situated behind the one corresponding to the hadronization process. As was discussed above in the consistent approach one should use the spacelike hypersurface to switch to the hadronic cascade. For the present analysis, in the case of hydrokinetic switching we use the $\sigma_{\text{sw}} : \tau = \tau_{\text{sw}} = \text{const}$ hypersurface, which is completely spacelike. However, other choices for switching spacelike hypersurface are also possible.

The hypersurface of chemical freeze-out, which is the matching hypersurface in pure "hybrid" scenario, is typically non-space-like, so the explicit parametrization of the hypersurface $\tau(\vec{r}_T)$ can be double-valued, as well as the parametrization $r_T(\tau, \phi)$. To escape multivalued functions one may utilize these different parametrizations in different sectors of the freeze-out hypersurface. In the case of the pure "hybrid" model it leads to the different representations for the distribution functions (4) for MC generation in different sectors of the hypersurface,

$$\frac{d^6 N_i}{d\tau\, d\eta\, d\phi\, dy\, dp_T\, d\phi_p} = F_i(\tau, \eta, \phi, y, p_T, \phi_p), \qquad (8)$$

if the explicit dependence $r_T = r_T(\tau)$ is assumed, or

$$\frac{d^6 N_i}{dr_T\, d\eta\, d\phi\, dy\, dp_T\, d\phi_p} = F_i(r_T, \eta, \phi, y, p_T, \phi_p), \qquad (9)$$

if another form $\tau = \tau(r_T, \phi)$ is used. For the isochronic switching procedure in the hydrokinetic approach, based on Eq. (5), only the form Eq. (9) is used.

Once the distribution function F on the switching hypersurface is known, we proceed with the standard (for present event generators) method of Monte Carlo event generation for input to UrQMD. First, one needs to calculate the maximum value of the distribution functions and the mean multiplicities of each sort of hadron in one event. Then, in each event we randomly generate the exact number of each sort of particle in a given rapidity interval according to Poisson distribution, such that the average multiplicity over a large set of events yields the mean multiplicity in the hydrokinetic approach at the chosen isochronic hypersurface. Then coordinates and momenta of each particle are generated randomly according to the distributions (4) or (5). To simplify the procedure of generation, the accept-reject algorithm is used, which means the following, e.g., in the case of distribution (8): We generate the random set of coordinates $x_r = \{\tau, \eta, \phi\}$ and momenta $p_r = \{y, p_T, \phi_p\}$ and a random variable a in interval $a \in [0, \ldots, F_{\text{max}}]$, where F_{max} is the maximal value of distribution (8). Then, we compare the value of distribution in the given point $F_r = F_i(x_r, p_r)$. If $a < F_r$, then the particle coordinate and momentum set are accepted; otherwise it is rejected, and the new random iteration is made. In this way, we generate in each event the coordinates and momenta of all particles with $|\eta_s| < 2$ and $|y| < 2$ intervals, which are wide enough to study particle production at midrapidity.

The generated set of particles is then used as input for UrQMD code [29], which computes further elastic and inelastic collisions and decays of unstable hadrons. Finally, the output of UrQMD—which is also a set of particle positions and momenta—is analyzed to obtain physical results of the model.

III. THE OBSERVABLES IN THE MODEL

The azimuthally averaged transverse momentum spectra,

$$\frac{dN}{2\pi p_T\, dp_T\, dy},$$

is calculated in the direct way from a generated event ensemble. When comparing to experimental data, we retain or neglect the feed-down from weak decays in accordance with experimental procedure.

In the described Monte Carlo procedure of event generation, the elliptic flow coefficients are calculated in the model in a "standard" way, according to

$$v_2 = \langle \cos 2(\phi_p - \Psi_{\text{RP}}) \rangle = \left\langle \frac{p_x^2 - p_y^2}{p_x^2 + p_y^2} \right\rangle, \qquad (10)$$

where the brackets correspond to the mean value over the particles from a given event ensemble (in a given p_T bin, for p_T-differential v_2). The procedure of reaction plane constructing is described in Sec. II A 1.

For femtoscopy analysis, we first calculate the three-dimensional two-pion correlation function as a function of relative momentum $\vec{q} = \vec{p}_1 - \vec{p}_2$ for each k_T bin, where $k_T = (p_1 + p_2)/2$ is the average momentum of the pion pair. Following the experimental cuts (which are somewhat different for the STAR, PHENIX, and ALICE collaborations), we consider pions in the central pseudorapidity region $|\eta| < 0.5$. To calculate the correlation function, we use the same technique as in our previous studies in the FASTMC event generator [34]. Namely, the correlation function for bosons in the Monte Carlo procedure is calculated according to

$$C(\vec{q}) = \frac{\sum_{i \neq j} \delta_\Delta(\vec{q} - p_i + p_j)[1 + \cos(p_j - p_i)(x_j - x_i)]}{\sum_{i \neq j} \delta_\Delta(\vec{q} - p_i + p_j)},$$

$$(11)$$

where $\delta_\Delta(x) = 1$ if $|x| < \Delta p/2$ and 0 otherwise, with Δp being the bin size in histograms. We decompose the relative momentum $\vec{q}$ into $(q_{\text{out}}, q_{\text{side}}, q_{\text{long}})$ projections and preform analysis in the longitudinal center of mass system (LCMS), where the mean longitudinal momentum of the pair vanishes.

Evaluation according to Eq. (11) is done with the help of 3D histograms, implemented in ROOT library classes [35], and two separate histograms are used to calculate the numerator and denominator of Eq. (11), which are divided to get the correlation function. We fit the resulting correlation function with the Bertsch-Pratt parametrization:

$$C(q) = 1 + \lambda \exp\left(-R_{\text{out}}^2 q_{\text{out}}^2 - R_{\text{side}}^2 q_{\text{side}}^2 - R_{\text{long}}^2 q_{\text{long}}^2\right).$$
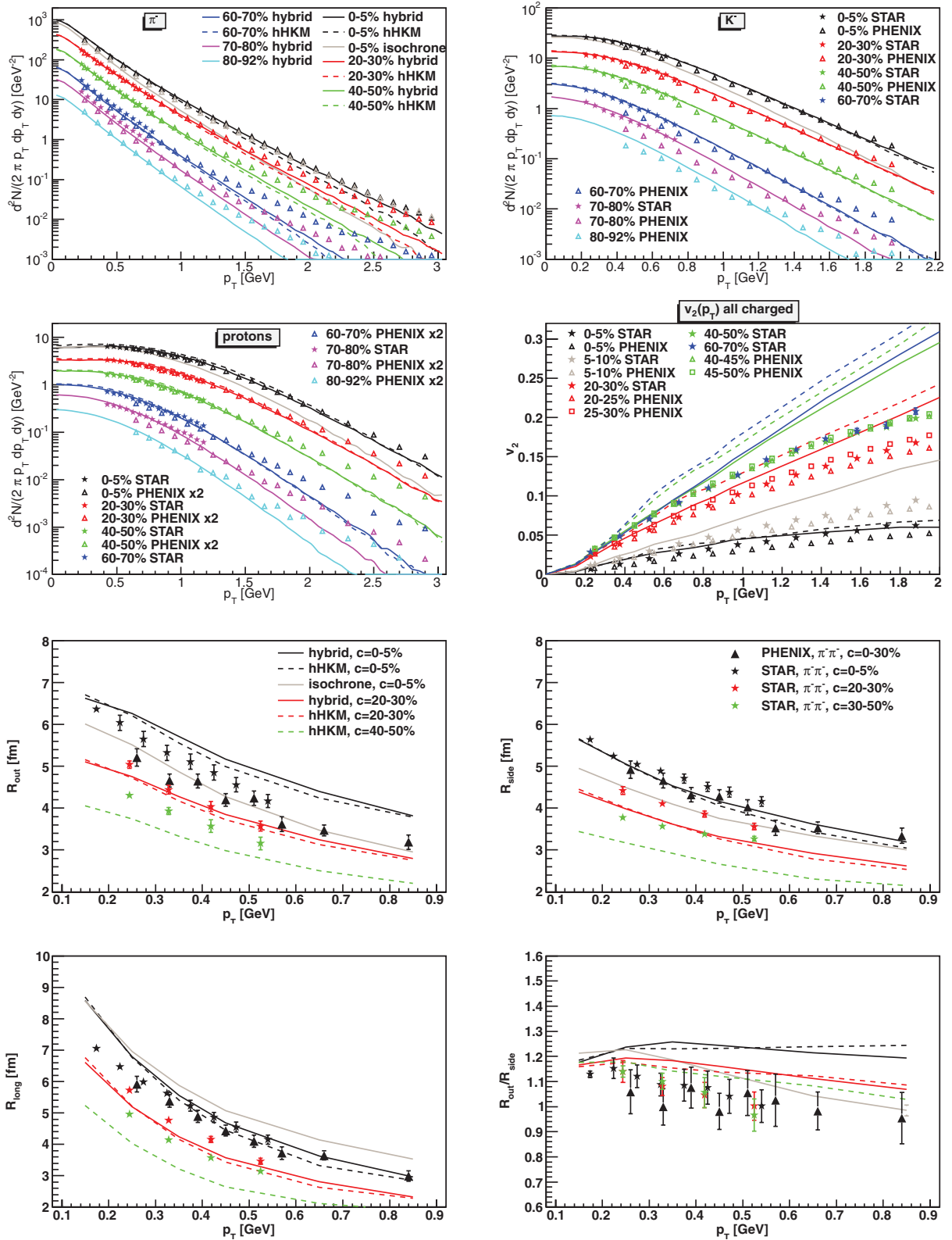
FIG. 2. (Color online) π^-, K^- and proton spectra and elliptic flow of all charged hadrons at midrapidity for 200-A GeV RHIC energy and different centrality classes (top) and HBT radii of π^- pairs for most central events, calculated in different models and compared to experimental data from the STAR [39–41] and PHENIX [42–44] collaborations. Note that proton PHENIX spectra is multiplied by the factor 2 (see text). Dashed lines correspond to the hydrokinetic procedure of matching (hHKM), while solid lines stand for the "hybrid" model case. The results for the "hybrid-isochronic" model are presented for central $c = 0\%$–5% events with a gray solid line. The ICs used: $\tau_0 = 0.1$ fm/c with zero initial transverse flow and the MC-Glauber profiles for initial entropy density.

Oowing to longitudinal boost invariance and approximate azimuthal symmetry for the most central collisions that we consider for the present HBT studies, the cross terms R_{os}^2, R_{sl}^2, and R_{ol}^2 are neglected.

A. The results for RHIC

The model parameters for MC-Glauber ICs are defined as follows. We consider the three switching procedures between hydrodynamics and the hadronic cascade. In the "hybrid" model the chemical freeze-out isotherm with temperature T_{ch} (defined below) serves as the switching hypersurface. In "hybrid-isochronic" model the switch of hydrodynamics to the UrQMD cascade is implemented at the isochronic hypersurface $\tau_{sw} = $ const, and τ_{sw} is defined from the requirement that the isochronic hypersurface touches the chemical freeze-out isotherm at $r = 0$: $T(\tau_{sw}, r = 0) = T_{ch}$. In the hydrokinetic procedure the switching hypersurface is the same isochronic one, but at time $\tau < \tau_{sw}$ the evolution is described by the hydrokinetic but not not pure hydrodynamics. The MC-Glauber ICs are attributed to the starting time $\tau_0 = 0.1$ fm/c in all the scenarios. The basic results are related to zero initial transverse flow.

The normalization constant C for the initial entropy density in Eq. (2) is defined by the all charged particle multiplicity in most central collisions $c = 0\%-5\%$ and is fixed for the given collision energy. The same concerns the parameter δ that defines the binary collision contribution according to Eq. (2). For RHIC $\delta = 0.14$. We also fix the parameters of chemical freeze-out: $T_{ch} = 165$ MeV, $\mu_B = 28$ MeV, $\mu_S = 7$ MeV, $\mu_E = -1$ MeV, according to the analysis of particle number ratios from STAR in thermal model [36,37], and include contributions from weak decays to the proton spectrum to make correspondence with STAR procedure. Some of the resulting particle number ratios are shown in Table II. Note that in our hadron table we also include additional resonance states, e.g., $f_0(600)$, $f_0(980)$, $a_0(980)$, and high mass resonances with $m > 2$ GeV, followed by the recent compilation from Particle Data Group [38]. $f_0(600)$ is observed as a broad resonance structure, with very little knowledge about its decay channels and branching ratios. However, these resonances contribute to both final pion and (less) proton yields [36]; thus, modifying particle number ratios, in particular, improves (anti)proton yields at RHIC.

1. The yields, spectra, v_2, and femtoscopy

We focus first on the description of the top RHIC Au + Au data in the hHKM model, which is shown in Fig. 2.

TABLE II. Identified hadron yields measured by STAR collaboration [39] for most central (0%–5%) Au + Au collisions at top RHIC energy, compared to hHKM calculations.

	N_{π^-}	N_{K^-}	N_p	$N_{\bar{p}}$
STAR	327 ± 33	49.5 ± 7.4	34.7 ± 6.2	26.7 ± 4.0
hHKM	330	47.3	29.9	20.5

It is known that even for the most central Au + Au collisions STAR and PHENIX proton multiplicities differ by a factor of ≈ 2, pion multiplicities by more than 15%, and these discrepancies rise from central to peripheral centrality classes; see Fig. 2. Within our model this difference cannot be fully reproduced by switching on/off weak contributions only; e.g., to reach lower pion multiplicity at PHENIX one also has to decrease initial energy density. We choose ICs in the model to reproduce the STAR multiplicities, but compare the results with the spectra and HBT radii measured by both collaborations. Because transverse momentum spectra of identified hadrons are measured in a wide p_T range only by PHENIX, we multiply the PHENIX proton spectrum by the factor 2 to better compare its shape with the STAR points and the hHKM calculations. From Fig. 2 it is seen that the kaon multiplicity is overpredicted in hHKM for noncentral events if compared to the PHENIX data, which could be a sign of the incomplete equilibration of strangeness in peripheral collisions [45]. However, this effect is not seen when one compares results with the STAR kaon data.

In the middle row of Fig. 2 we compare the elliptic flow coefficients in full hHKM and "hybrid" scenarios with the STAR [40] and PHENIX [43] results for all charged hadrons, obtained with event-plane method. In addition, in Fig. 3 we present elliptic flow of charged pions, kaons, and (protons + antiprotons), calculated with the same parameters as for Fig. 2, and compared to $v_2\{2\}$ for charged pions, kaons, and antiprotons from STAR (using a two-particle cumulant method). This calculation is done only for the centrality $c = 20\%-30\%$, because a considerably bigger set of events must be used for this observable. One can see some overestimate of the data for v_2 coefficients; it is because we use ideal hydrodynamics, but not a viscous one.

The comparison of interferometry radii, calculated in the model with the experimental data, is shown in the bottom of Fig. 2. Note that PHENIX presented its results for the 0%–30% centrality bin, which corresponds to a smaller average multiplicity than the 0%–5% STAR bin, thus PHENIX radii lie slightly below ones calculated by STAR; in our model we
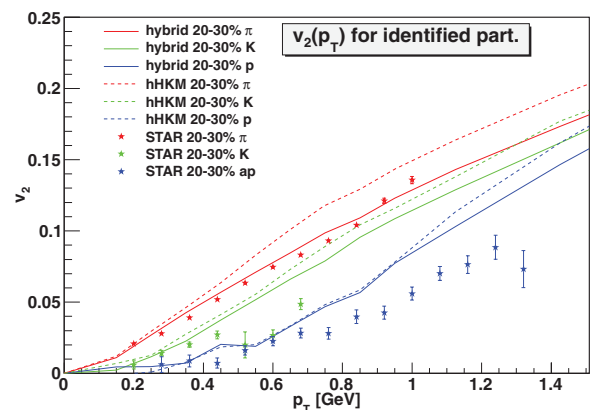

FIG. 3. (Color online) Elliptic flow of $\pi^\pm$, $K^\pm$ and (anti)protons at top RHIC energy and centrality $c = 20\%-30\%$, calculated in the hHKM and "hybrid" models with the same parameters as in Fig. 2 and compared to the STAR data [40].

observe the same tendency with average ICs for the 0%–30% centrality.

From Figs. 2 and 3 one can conclude that both the hHKM and the "hybrid" models describe the data quite satisfactory, except v_2 for very noncentral collisions (where the viscosity should play an important role and reduces elliptic flow) and HBT radii for 40%–50% centrality, which are clearly underestimated. The shear viscosity should also reduce the R_{out}/R_{side} ratio because it enhances the transverse flow. As for the "hybrid-isochrone" model, it fails to describe the shape of pion, kaon, and proton transverse spectra, v_2, and long-, side-, and out-interferometry radii. The main difference between the first two (hHM, hybrid) and hybrid-isochrone scenarios is that the first two matching procedures do not use the local equilibrium particle distribution functions as input for UrQMD cascade at the space-time regions where the system should be far from equilibrium. The peripheral regions at isochronic hypersurface are spatially and temporally distant from the freeze-out isotherm and have rather small temperatures, and in this transition area the finite and rapidly expanding system cannot be described hydrodynamically: The free-streaming regime of particle propagation already starts there. However, such a system can be described with the hydrokinetic approach. In what follows we consider only hHKM and "hybrid" models.

B. The results for LHC

We now move to LHC energy to inspect now well the hHKM and "hybrid" models fit to 2.76-TeV LHC Pb + Pb collisions. First we have to account for the corresponding increase of the initial entropy production at the LHC energy by changing the normalization constant C in Eq. (2) of the initial energy density profile; the parameter δ is chosen to be 0.08 [21] for LHC energy. With bigger initial energy density, hydrodynamic evolution evidently leads to larger effective volume at the chemical freeze-out hypersurface, as well as to bigger transverse flow; see Fig. 4. The second modification is related to the chemical composition at freeze-out: According to approximate particle-antiparticle symmetry at $\sqrt{s} = 2.76$ TeV energy, confirmed by ALICE data [46], we set all chemical potentials to zero: $\mu_B = \mu_Q = \mu_s = 0$.

1. Yields and particle-number ratios

Let us start with the particle-number ratios obtained in the hHKM model for LHC energy. In the simulations we also observe antiparticle/particle symmetry in π^-/π^+, K^-/K^+, $\bar{p}/p$ ratios, which are all close to 1. From the spectra plots in Fig. 5 one can conclude that (anti)proton multiplicity at midrapidity in the hHKM model is only slightly overestimated. Indeed, the nontrivial particle number ratios at midrapidity are shown in Table III. To understand which factors contribute to successful description of particle-number ratios at LHC (and in particular the p/π ratio), let us calculate hadron yields in different scenarios of evolution at the post-chemically equilibrated phase, while keeping the same ICs and chemical composition at chemical freeze-out. In this subanalysis we look at the most central collisions, where rescattering effects in
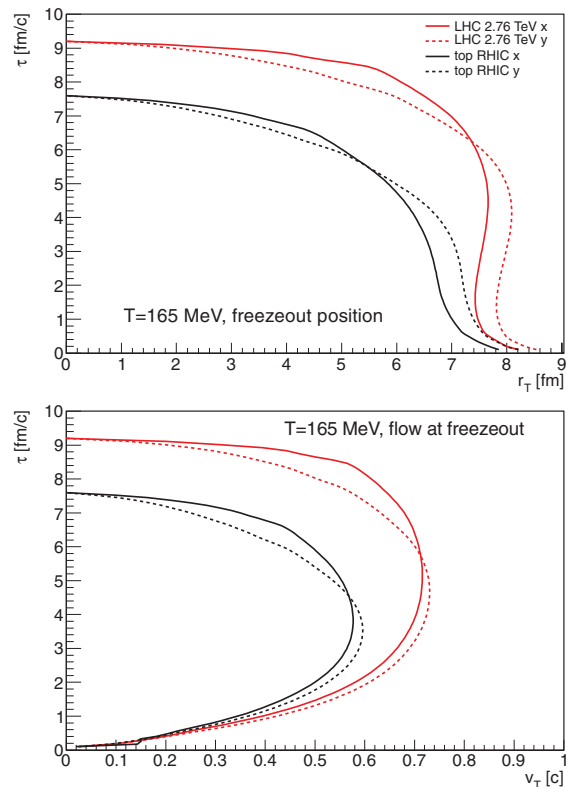

FIG. 4. (Color online) Chemical freeze-out hypersurface profiles and transverse flows at the chemical freeze-out position in the hHKM model. Profiles are made in the in-plane direction (solid lines) and the out-of-plane direction (dashed lines) for top RHIC (black) and 2.76-TeV LHC (red) $A + A$ collisions. ICs are taken from the MC-Glauber model.

cascade—via UrQMD code—should be most prominent. From Table III one can see that both pion and proton yields are minimal for the "thermal model" scenario, where only resonance decays are enabled. Involvement of UrQMD to calculate both elastic and inelastic scatterings [except for baryon-antibaryon annihilation, turned off with CTOption(19) = 1] increases somewhat both pion and λ yields. Finally, switching on $B\bar{B}$ annihilation suppresses baryon yields, and at the same time increases pion yield, thus lowering the p/π ratio to the value 0.052, which is quite close to the one measured by ALICE [46]. Thus, one can conclude that annihilation processes in UrQMD are essential for successful reproduction of the p/π ratio at

TABLE III. Particle multiplicities and particle number ratios, calculated within the hHKM model for most central (0%–5%) Pb + Pb collisions with $\sqrt{s} = 2.76$ TeV in differen scenarios of particle production: full scenario (hydro + UrQMD), full-$B\bar{B}$ (baryon-antibaryon annihilator switched off in UrQMD), and thermal model (kinetic phase with resonance decays only).

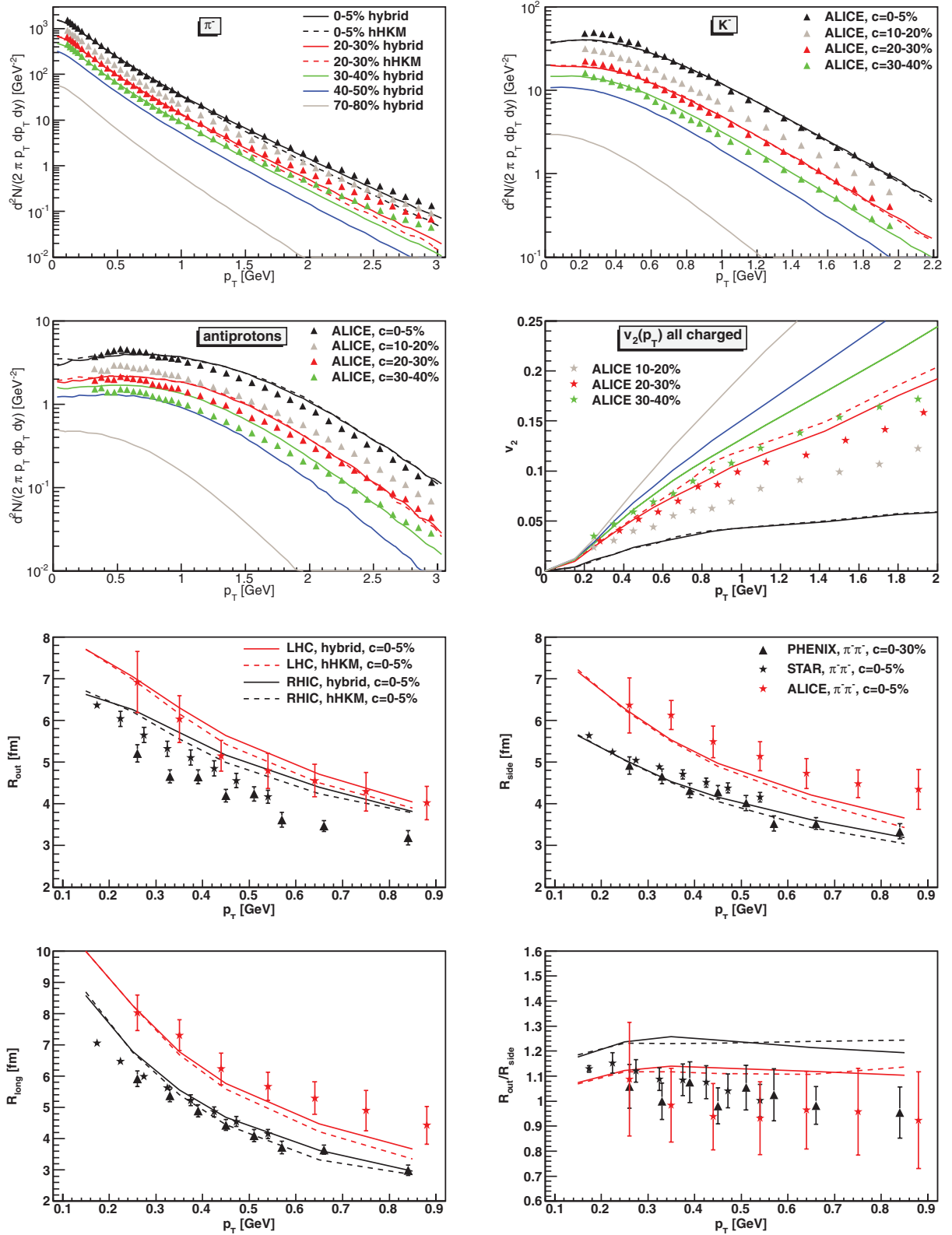|	N_π	N_K	N_p	N_Λ	p/π	K/π	Λ/π
Full	775	123	40.5	20	0.052	0.158	0.026
Full-$B\bar{B}$	716	114	50.5	24	0.072	0.159	0.034
Thermal	679	127	54	20.3	0.08	0.188	0.03

FIG. 5. (Color online) π^-, K^- and proton spectra and elliptic flow of all charged hadrons at midrapidity for 2.76-TeV LHC energy and different centrality classes (top) and HBT radii of π^- pairs for most central events, calculated in the hHKM model and compared to experimental data from ALICE [1,3,46]. Dashed lines correspond to hydrokinetic procedure of matching, while solid lines stand for the "hybrid" model case. Corresponding HBT radii for top RHIC energy are shown for comparison purposes. Note that calculations for $c = 10\%-20\%$ are not provided, but the v_2 coefficient for $c = 0\%-5\%$ is presented instead as prediction.

the LHC energy. When going to noncentral collisions, the p/π ratio slightly increases up to 0.058 for 20%–30% centrality (consistently with ALICE data), which should be the result of fewer inelastic processes owing to decreased effective volume at the hadronization hypersurface. Because charged hadron density at midrapidity for 20%–30% central Pb + Pb collisions at 2.76 TeV is close to the one for most central collisions at top RHIC energy, one can also conclude that inelastic processes in the cascade play a similar role also at RHIC, modifying particle number ratios and, in particular, decreasing the p/π ratio. It is worth noting that the value of the effect depends on the dynamics of the fireball that defines a duration of the afterburn stage and so can differ at RHIC and LHC energies.

2. Spectra, elliptic flow, and femtoscopy

In Fig. 5 we show the comparison model/experiment for 2.76-TeV LHC energy. The experimental data are related to elliptic flow coefficients from the four-particle cumulant method, $v_2\{4\}$ [1] and interferometry radii to the most central events measured by the ALICE Collaboration [3]. In addition, as for the RHIC case, in Fig. 6 we compare the elliptic flow $v_2\{2\}$ of charged pions, kaons and antiprotons for the centrality 10%–20%, measured by ALICE [47]. On the last plot, the experimental points are somewhat above the hHKM calculations, and the probable source of the difference is the two-particle cumulant method, which give systematically bigger elliptic flow than the four-particle cumulant method used for the analysis of the elliptic flow of all charged hadrons. To compare with the experimental antiproton spectrum from ALICE, we exclude all feed-downs from weak decays, except for $\bar{\Sigma}^+$. As a result, we observe some difference compared to ALICE for the mass dependence of the effective temperature (inverse slope) of the transverse momentum spectrum: The resulting antiproton and kaon spectra are too flat in the model, while the pion spectrum is reproduced much better in a wide p_T region. The reason for such a mismatch could be that the imitation of the viscous effects by the initial transverse

FIG. 6. (Color online) Elliptic flow of $\pi^\pm$, $K^\pm$ and (anti)protons at top 2.76-TeV LHC energy and centrality $c = 30\%-40\%$, calculated in the hHKM model with the same parameters as in Fig. 5 and compared to ALICE data [47].

flow is not so effective at LHC than at RHIC because of a more protracted (viscous) hydrodynamics stage. Concerning interferometry results, in hHKM we get systematically lower R_{side} and R_{long} radii than the ALICE data for larger p_T; however, they are within the experimental error bars almost in all p_T regions. Note that the rise of interferometry volume observed by the ALICE collaboration is well reproduced in hHKM (see also Ref. [14]). Because we keep untouched the main model parameters when passing from RHIC to LHC energies, except for a general normalization for increased dN/dy, contribution from binary collisions, and the baryonic chemical potentials at freeze-out, one can conclude that the soft physics at RHIC and LHC is similar.

C. Possible corrections to the basic results

The above results are presented for perfect fluid dynamics of quark-gluon plasma and nonequilibrium evolution of hadronic gas after the chemical freeze-out. As is known, quantum theory gives the limitation on the shear viscosity coefficient η, more exactly, on the minimal ratio $\frac{\eta}{s} = \frac{1}{4\pi}$, where s is entropy density. The inclusion of the shear viscosity in the boost-invariant hydrodynamic models affects the final hydrodynamic flow in the following way: It increases the radial and decreases elliptic flows.

In this work we do not utilize viscous hydrodynamics. However, in this section we try to demonstrate the influence of the above-mentioned effects on observed transverse spectra, elliptic flows, and HBT. Of course, the conservation laws have to be taken into account to see reliable correlation in modifications of different kinds of observables. For this aim we use our model with modified ICs that affect the final flow in the above-mentioned way. We found that the artificial addition of a small initial transverse velocity with profile (3) can serve for this aim. In this case the pressure gradient will drop faster in all directions and this reduces an efficiency of the transformation of the anisotropy of initial pressure gradient into the final flow anisotropy [7]. Formally, when $\mathbf{v} \to \mathbf{v} + \mathbf{v}_{\text{rad}}$, the anisotropy parameter $\epsilon_v = \langle v_x - v_y \rangle / \langle v_x + v_y \rangle$ drops.

From the comparison with the LHC experimental data in Fig. 7 one can see some improvement of the behavior for all the observables, when small initial flow is included with the average value being $\langle v_{\text{T,ini}} \rangle = 0.014$–$0.018$. Namely, the effective temperature of the single-particle transverse spectra at large p_T increases, while the v_2-coefficient decreases and $R_{\text{out}}/R_{\text{side}}$ ratio becomes lower.

These "viscouslike" corrections bring the hope that the good description of the RHIC and LHC experiments can be reached within the HKMs based on viscous hydrodynamics. This will be the next step in our study.

IV. CONCLUSIONS

We present a consistent description of the transverse momentum spectra for the most abundant hadrons (π, K, p), elliptic flow coefficients, and interferometry radii for central and noncentral collisions at the top RHIC and LHC energies in the hHKM. The latter provides the correct matching
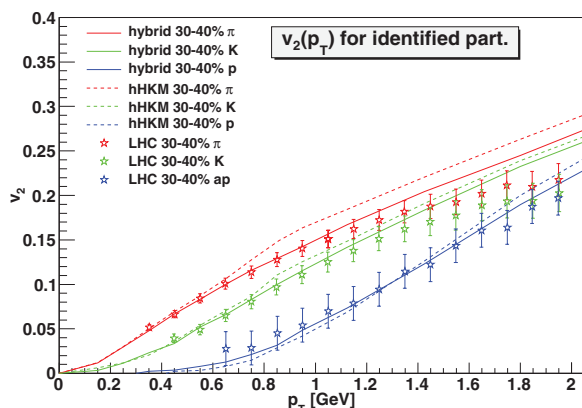
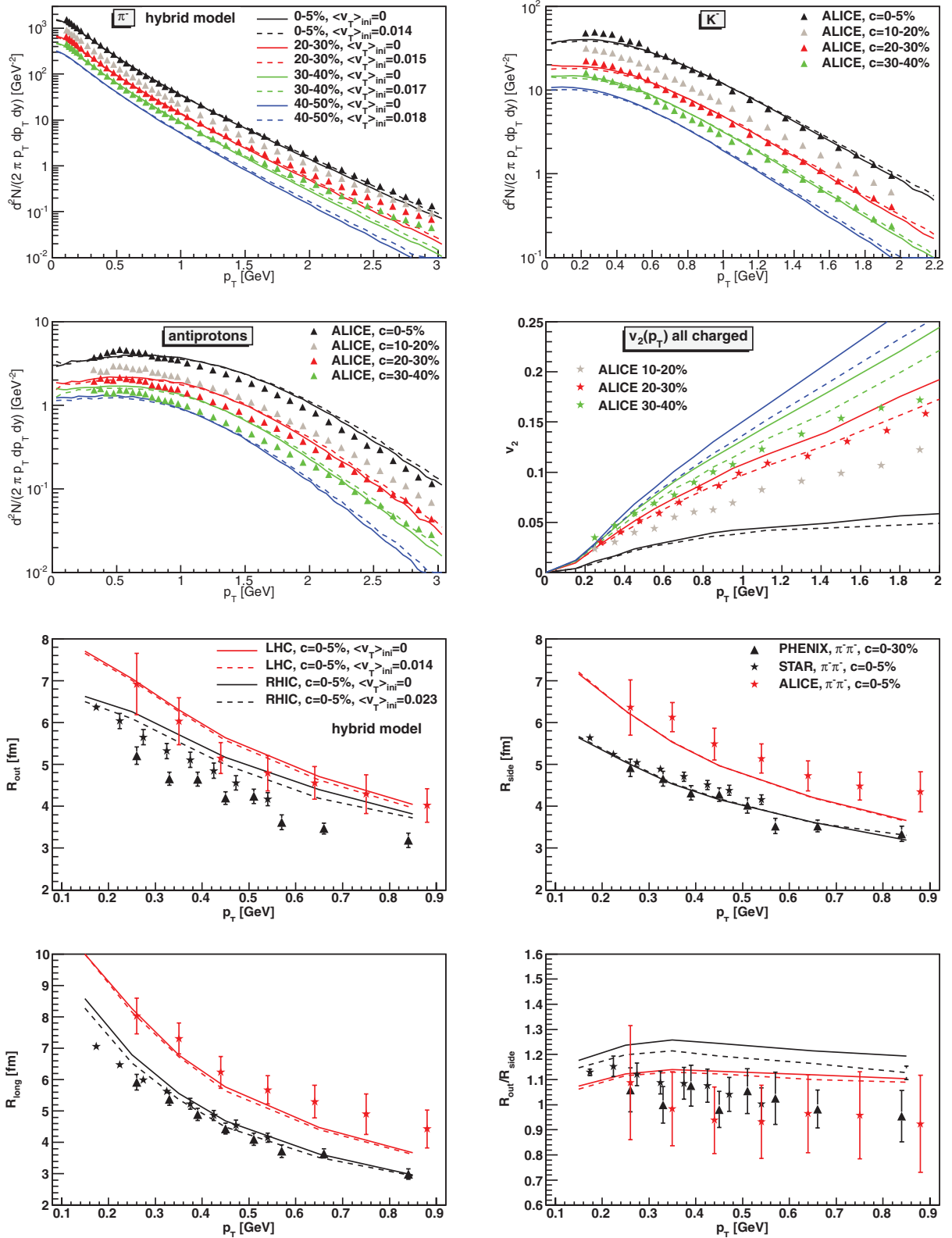FIG. 7. (Color online) π^-, K^- and proton spectra and elliptic flow of all charged hadrons at midrapidity for 2.76-TeV LHC energy and different centrality classes (top) and HBT radii of π^- pairs for most central events, calculated in the "hybrid" model and compared to experimental data from ALICE [1,3,46]. Solid lines correspond to IC without transverse flow, while dashed lines stand for small initial transverse flows, $\langle v_T \rangle = 0.014$–$0.018$. Corresponding HBT radii for the top RHIC energy are shown for comparison purposes for the basic case without initial transverse flow. Note that calculations for $c = 10\%-20\%$ are not provided, but the v_2 coefficient for $c = 0\%-5\%$ is presented instead as prediction.

of decaying hadron matter evolution with hadronic UrQMD cascade at isochronic (or spacelike in general) hypersurface. The results are compared with ones obtained at the different matching procedures in hybrid models with the same ICs. It is found that the matching of hydrodynamics with cascade at the chemical freeze-out hypersurface gives the close results to hHKM, while the results are essentially different from both of these models and from experimental data when the matching of thermally and chemically equilibrated hydrodynamic systems with UrQMD happens at the isochronic hypersurface.

The ICs allowing simultaneous description of the soft observables in ultrarelativistic $A + A$ collisions are associated with the MC-Glauber initial entropy density distribution with mixed contributions from wounded nucleon density and density of binary scatterings. One can see the satisfactory description of the RHIC and LHC data within perfect hydrodynamics for the QGP phase, except for some overestimation of v_2 coefficients and R_{out}/R_{side} ratios caused, probably, by neglect of the shear viscosity. As is known the latter increases the final transverse flow and damps the elliptic flows. Qualitatively, similar effects can be reached by artificial inclusion of small but nonzero initial transverse flow. We demonstrate that such an imitation of the shear viscosity indeed improves the v_2 coefficients and R_{out}/R_{side} ratios.

The hadron yields and particle number ratios for most abundant hadrons measured by ALICE are also well described and explained in the model. The contributions of different processes at the hadronic cascade stage to the final hadron yields are found.

Note that the most of the parameters fixed from agreement with RHIC data are applied also for the description of 2.76-TeV Pb + Pb LHC collisions with different centrality classes. In fact, the only changes are the normalization of initial entropy density distribution, contribution from binary collisions and baryonic chemical potentials at chemical freeze-out, which become zero. Then pion, kaon, and (anti) proton spectra, p_T-differential elliptic flow coefficients, and HBT radii are reproduced well also at LHC. It is evidence of the similarity of the soft physics at the RHIC and LHC energies.

As the next step it is planned to include some missing features of the hydrokinetics into future versions of the model, namely the prethermal dynamics and viscosity.

[1] K. Aamodt *et al.* (ALICE Collaboration), Phys. Rev. Lett. **105**, 252302 (2010).

[2] N. Armesto (editor) *et al.*, J. Phys. G **35**, 054001 (2008).

[3] K. Aamodt *et al.* (ALICE Collaboration), Phys. Lett. B **696**, 328 (2011).

[4] M. Chojnacki, W. Florkowski, W. Broniowski, and A. Kisiel, Phys. Rev. C **78**, 014905 (2008).

[5] I. A. Karpenko and Y. M. Sinyukov, Phys. Lett. B **688**, 50 (2010).

[6] P. F. Kolb, J. Sollfrank, and U. Heinz, Phys. Rev. C **62**, 054909 (2000); P. F. Kolb *et al.*, Phys. Lett. B **500**, 232 (2001).

[7] Yu. M. Sinyukov, Acta Phys. Pol. B **37**, 3343 (2006).

[8] S. V. Akkelin, Y. Hama, Iu. A. Karpenko, and Yu. M. Sinyukov, Phys. Rev. C **78**, 034906 (2008).

[9] Yu. M. Sinyukov, A. V. Nazarenko, and Iu. A. Karpenko, Acta Phys. Pol. B **40**, 1109 (2009); M. Gyulassy, Iu. Karpenko, A. V. Nazarenko, and Yu. M. Sinyukov, Braz. J. Phys. **37**, 1031 (2007).

[10] W. Broniowski, W. Florkowski, M. Chojnacki, and A. Kisiel, Phys. Rev. C **80**, 034902 (2009).

[11] S. Pratt, Nucl. Phys. A **830**, 51c (2009).

[12] Iu. A. Karpenko and Yu. M. Sinyukov, Phys. Rev. C **81**, 054903 (2010).

[13] Yu. M. Sinyukov, S. V. Akkelin, and Y. Hama, Phys. Rev. Lett. **89**, 052301 (2002).

[14] Iu. A. Karpenko and Yu. M. Sinyukov, J. Phys. G **38**, 124059 (2011).

[15] K. Werner, Iu. Karpenko, T. Pierog, M. Bleicher, and K. Mikhailov, Phys. Rev. C **82**, 044904 (2010).

[16] P. Bozek, Phys. Rev. C **85**, 034901 (2012).

[17] P. Bozek, Acta Phys. Pol. B **43**, 689 (2012).

[18] D. Kharzeev and M. Nardi, Phys. Lett. B **507**, 121 (2001).

[19] W. Broniowski, M. Rybczynski, and P. Bozek, Comput. Phys. Commun. **180**, 69 (2009).

[20] B. B. Back *et al.* (PHOBOS Collaboration), Phys. Rev. C **65**, 061901 (2002).

[21] T. Hirano, P. Huovinen, and Y. Nara, Phys. Rev. C **84**, 011901 (2011).

[22] S. V. Akkelin and Yu. M. Sinyukov, Phys. Rev. C **81**, 064901 (2010).

[23] M. Laine and Y. Schroder, Phys. Rev. D **73**, 085009 (2006).

[24] F. Karsch, PoS **CPOD07**, 026 (2007).

[25] P. Huovinen and P. Petreczky, Nucl. Phys. A **837**, 26 (2010).

[26] C. Shen, U. Heinz, P. Huovinen, and H. Song, Phys. Rev. C **82**, 054904 (2010).

[27] M. Cheng *et al.*, Phys. Rev. D **77**, 014511 (2008).

[28] A. Bazavov *et al.*, Phys. Rev. D **80**, 014504 (2009).

[29] S. A. Bass *et al.*, Prog. Part. Nucl. Phys. **41**, 255 (1998); M. Bleicher *et al.*, J. Phys. G **25**, 1859 (1999).

[30] F. Cooper and G. Frye, Phys. Rev. D **10**, 186 (1974).

[31] Y. M. Sinyukov, Z. Phys. C **43**, 401 (1989).

[32] K. A. Bugaev, Phys. Rev. Lett. **90**, 252301 (2003).

[33] K. A. Bugaev, Nucl. Phys. A **606**, 559 (1996).

[34] N. S. Amelin, R. Lednicky, T. A. Pocheptsov, I. P. Lokhtin, L. V. Malinina, A. M. Snigirev, Iu. A. Karpenko, and Yu. M. Sinyukov, Phys. Rev. C **74**, 064901 (2006).

[35] ROOT Data Analysis Framework, http://root.cern.ch/drupal/.

[36] A. Andronic, P. Braun-Munzinger, and J. Stachel, Acta Phys. Pol. B **40**, 1005 (2009).

[37] J. Manninen and F. Becattini, Phys. Rev. C **78**, 054901 (2008); F. Becattini and J. Manninen, J. Phys. G **35**, 104013 (2008).

[38] K. Nakamura *et al.* (Particle Data Group), J. Phys. G **37**, 075021 (2010), and 2011 partial update for the 2012 edition.

[39] J. Adams *et al.* (STAR collaboration), Phys. Rev. Lett. **92**, 112301 (2004).

[40] J. Adams *et al.* (STAR Collaboration), Phys. Rev. C **72**, 014904 (2005).

[41] J. Adams *et al.* (STAR Collaboration), Phys. Rev. C **71**, 044906 (2005).

[42] S. S. Adler *et al.* (PHENIX Collaboration), Phys. Rev. C **69**, 034909 (2004).

[43] A. Adare *et al.* (PHENIX Collaboration), Phys. Rev. Lett. **105**, 062301 (2010).

[44] S. S. Adler *et al.* (PHENIX Collaboration), Phys. Rev. Lett. **93**, 152302 (2004).

[45] J. Cleymans, B. Kampfer, M. Kaneta, S. Wheaton, and N. Xu, Phys. Rev. C **71**, 054901 (2005).

[46] R. Preghenella for the ALICE Collaboration, Acta Phys. Pol., B **43**, 555 (2012).

[47] M. Krzewicki (ALICE Collaboration), J. Phys. G **38**, 124047 (2011).